A Low-Power Demodulator for LoRa Backscatter Systems With Frequency-Amplitude Transformation

Xiuzhen Guo, *Member, IEEE, ACM*, Yuan He, *Senior Member, IEEE, Member, ACM*, Jing Nan, *Member, IEEE*, Jiacheng Zhang, *Student Member, IEEE*, Yunhao Liu, *Fellow, IEEE, ACM*, and Longfei Shangguan, *Member, IEEE*

***Abstract*— The radio range of backscatter systems continues growing as new wireless communication primitives are continuously invented. Nevertheless, both the bit error rate and the packet loss rate of backscatter signals increase rapidly with the radio range, thereby necessitating the cooperation between the access point and the backscatter tags through a feedback loop. Unfortunately, the low-power nature of backscatter tags limits their ability to demodulate feedback signals from a remote access point and scales down to such circumstances. This paper presents Saiyan, an ultra-low-power demodulator for long-range LoRa backscatter systems. Saiyan is based on an observation that a frequency-modulated chirp signal can be transformed into an amplitude-modulated signal using a differential circuit. Moreover, we redesign a LoRa backscatter tag which integrates Saiyan and a ring oscillator-based modulator. The LoRa backscatter tag enables re-transmission, rate adaption and channel hopping – three PHY-layer operations that are important to channel efficiency yet unavailable on existing long-range backscatter systems. We prototype Saiyan and the LoRa backscatter tag on two PCB boards and evaluate their performance in different environments. Results show that Saiyan achieves 3.5–5× gain on the demodulation range, compared with state-of-the-art systems. Our ASIC simulation shows that the power consumption of Saiyan and the LoRa backscatter tag are around 93.2 μW and 94.7 μW. Code and hardware schematics can be found at: https://github.com/ZangJac/Saiyan.**

***Index Terms*— Wireless networks, backscatter communication, LoRa, low-power demodulator.**

I. Introduction

THE proliferation of Internet of Things (IoT) applications brings about the increasingly dense deployments of various wireless radios [1], [2]. Now, backscatter radios have emerged as an ultra-low-power and economical alternative to active radios. The ability to communicate over long distances is critical to the practical deployment of backscatter systems, particularly in outdoor scenarios (*e.g.*, smart farm) where backscatter tags need to deliver their data to a remote access point regularly. Conventional RFID technology [3] functions within only a few meters and is not well suited for outdoor scenarios. To this end, the research community has proposed long-range backscatter approaches [4], [5], [6] that leverage Chirp Spreading Spectrum (CSS) modulation on LoRa [7], [8] to improve the signal resilience to noise, thereby extending the communication range. For instance, LoRa backscatter [6] allows tags to communicate with a source and a receiver separated by 475 m.

Fig. 1. Saiyan empowers the LoRa backscatter tag to demodulate feedback signals from a remote access point. The tag demodulates feedback signals and makes on-demand re-transmissions in the presence of packet loss.

However, existing long-range LoRa backscatter systems present a new challenge on packet delivery. The backscatter signals travel twice the link distance and suffer drastic attenuation as the link distance scales. They become very weak after traveling long distances, thereby causing severe bit errors and packet losses. Figure 2 shows the Bit Error Rate (BER) of PLoRa [4] and Aloba [5], two representative long-range LoRa backscatter systems. Evidently, the BER of both systems rises rapidly from less than 1% to over 50% as the tag is moved away from the transmitter (Tx). The receiver is almost unable to demodulate any backscatter signal once the tag is placed 20 m away from the transmitter. Considering that the backscatter tags are unaware of packet loss, each packet must be transmitted blindly for multiple times to lift the packet delivery ratio, which inevitably wastes precious energy and wireless spectrum and cause interference to other radios that work on the same frequency band.

To address these issues, we expect a *downlink* from the access point to the backscatter tag, through which the feedback signals (*e.g.*, asking for a packet re-transmission) can be delivered, thereby forming a *feedback loop*, as shown in Figure 1. We envision that such a feedback loop will bring opportunities to bridge the gap between long-range backscatter

Manuscript received 24 June 2023; revised 24 January 2024 and 6 April 2024; accepted 18 April 2024; approved by IEEE/ACM TRANSACTIONS ON NETWORKING Editor S. M. Kim. This work was supported by the National Science Fund of China under Grant 62202264, Grant 62394341, Grant 62394344, and Grant U21B2007. *(Corresponding author: Yuan He.)*

Xiuzhen Guo is with the College of Control Science and Engineering, Zhejiang University, Hangzhou 310058, China (e-mail: guoxz@zju.edu.cn).

Yuan He, Jiacheng Zhang, and Yunhao Liu are with the School of Software, Tsinghua University, Beijing 100084, China (e-mail: heyuan@mail.tsinghua.edu.cn; jingnan@ysu.edu.cn; yunhaoliu@gmail.com).

Jing Nan is with the School of Information Science and Engineering, Yanshan University, Qinhuangdao 066104, China (e-mail: jingnan@ysu.edu.cn).

Longfei Shangguan is with the Department of Computer Science, University of Pittsburgh, Pittsburgh, PA 15261 USA (e-mail: longfei@pitt.edu).

Digital Object Identifier 10.1109/TNET.2024.3396509

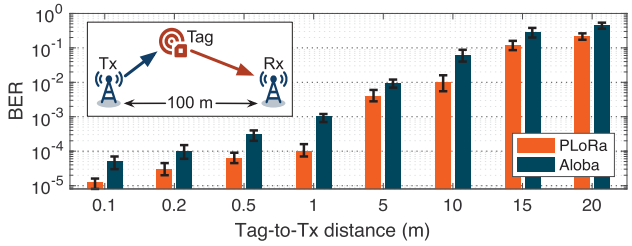

Fig. 2. BER of PLoRa [4] and Aloba [5] in different tag-to-transmitter settings. The BER of both systems rises dramatically with the increasing distance between the transmitter and the tag. We re-implement both systems on PCB.

communication and the growing packet loss rate, as reflected on the following aspects:

• *Making on-demand re-transmissions in the presence of packet loss*. The backscatter tag demodulates feedback signals from an access point and makes a re-transmission only if it is asked to do so. This reactive packet re-transmission can mitigate packet loss while improving power and channel efficiency.

• *Scheduling channel hopping to minimize interference*. The unlicensed band where the LoRa resides in is already over crowded. The access point monitors the wireless spectrum and notifies the backscatter tag to switch channels in the presence of in-band interference. As such, the channel utilization and packet delivery ratio can be improved effectively.

• *Adapting data rate to link condition*. The condition of backscatter links varies over time. The access point assesses each backscatter link and keeps the backscatter tag updated through the feedback loop. Each tag then adapts its data rate proactively to utilize the wireless link better.

In this paper, we propose Saiyan, a low-power demodulator for long-range LoRa backscatter systems. Saiyan is based on an observation that *a frequency-modulated chirp signal can be transformed into an amplitude-modulated signal using a differential circuit*. The amplitude of this transformed signal scales with the frequency of the incident chirp signal, thereby allowing us to demodulate a LoRa chirp by tracking the peak amplitude on its transformed counterpart without using power-intensive hardware, such as a down-converter and an ADC. To put this high-level idea into practice, the challenges in design and implementation must be addressed, as summarized below.

Frequency-amplitude transformation. The low-power nature of backscatter tags requires the differential circuit to be extremely low-power. Moreover, to support higher data rate, such a differential circuit should also be hyper-sensitive to the frequency variation of LoRa signals. However, the narrow bandwidth of LoRa signals (*e.g.*, 125/250/500 KHz) renders the conventional detuning circuits, such as RLC resonant circuit, inapplicable. In Saiyan, we instead repurpose the Surface Acoustic Wave (SAW) filter as a signal converter by leveraging its sharp frequency response (§II-A). To minimize the power consumption on demodulation, we further replace the power-consuming ADC with a well-designed double-threshold based comparator coupled by a proactive voltage sampler (§II-B).

Improving the demodulation sensitivity. Although the aforementioned vanilla Saiyan can demodulate LoRa signals with the minimum power consumption, its communication range is limited to 55 m because of the Signal-to-Noise Ratio (SNR) losses in both SAW filter and envelope detector. To extend the communication range, we introduce a low-power cyclic-frequency shifting circuit coupled with an Intermediate Frequency (IF) amplifier to simultaneously remove the noise while magnifying the signal power. This low-power circuit brings 11 dB SNR gain and doubles the demodulation range (§III-A). Furthermore, a low-power correlator is leveraged to extend the demodulation range further to 148 m (§III-B).

As an ultra-low-power peripheral, Saiyan can be integrated into a powerful LoRa backscatter tag with the uplink modulator. We redesign a LoRa backscatter tag ((§IV)), which integrates a ring oscillator-based, ultra-low power radio for the uplink modulator and the low-power Saiyan for the downlink demodulator. Hence, this LoRa backscatter tag enables re-transmission, channel hopping, rate adaption, *etc.*, PHY-layer operations that are important to channel efficiency yet unavailable on existing LoRa backscatter systems.

Implementation. We implement Saiyan on a 25 $mm\times20$ mm two-layer Printed Circuit Board (PCB) using analog circuit components and an ultra-low power Apollo2 MCU [9]. The Application Specific Integrated Circuit (ASIC) simulation shows that the power consumption can be reduced to 93.2 μW, which is affordable on an energy harvesting tag. We also implement the redesigned bi-directional LoRa backscatter tag on a 30 $mm\times22$ mm two-layer PCB using analog circuit components. The ASIC simulation shows that the power consumption of this LoRa backscatter tag can be reduced to 94.7 μW. The main contributions of this paper are summarized as follows:

• We simplify the standard LoRa demodulation from energy perspective and design the first-of-its-kind low-power LoRa demodulator that can run on an energy harvesting tag.

• We design a set of simple but effective circuits and algorithms, prototyping them on PCB board for system evaluation.

• We demonstrate that Saiyan outperforms the state-of-the-arts on power consumption, communication range, and throughput.

Roadmap. We introduce the design of Vanilla Saiyan and Super Saiyan in Section II and Section III, respectively. In Section IV, We integrate Saiyan and a ring oscillator-based uplink modulator into a redesigned bi-directional LoRa backscatter tag. We sketch the MAC layer design in Section V and introduce the implementation details in Section VI. Section VII presents the evaluation results. We review related works in Section VIII and discuss the limitation in Section IX. Section X concludes this paper.

II. Vanilla Saiyan

A LoRa symbol is represented by a chirp whose frequency grows linearly over time [10], [11], [12], as formulated below.

$$s(t) = Asin(2\pi f(t)t) \tag{1}$$

where A is the signal amplitude; $f(t) = F_0 + kt$ describes how the frequency of this chirp signal varies over time; F_0 is the initial frequency offset; k is the frequency changing rate. The frequency of a LoRa chirp wraps to 0 right after peaking BW—the bandwidth of LoRa. Different LoRa chirps peak the

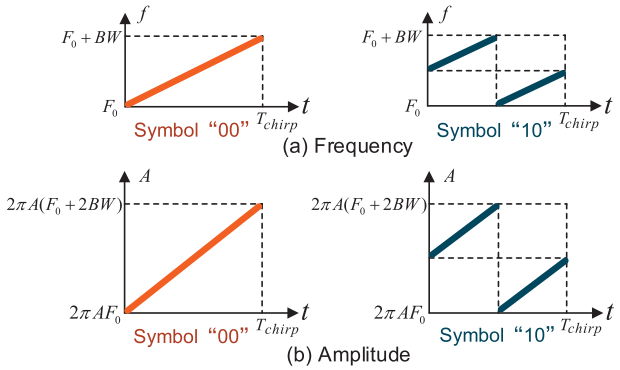

Fig. 3. LoRa symbols before and after frequency-amplitude transformation. (a) Different LoRa symbols in the frequency domain. (b) The amplitude of LoRa symbols after frequency-amplitude transformation.

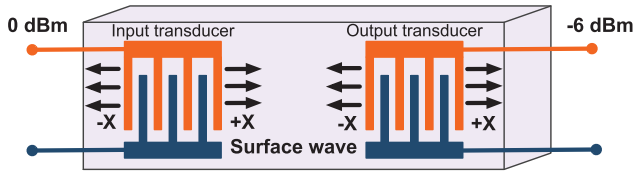

Fig. 4. Diagram of the SAW filter. The SAW filter converts electrical signal into acoustic signal and then back through two inter-digital transducers.

frequency BW at different time due to the difference in their initial frequency offset, as shown in Figure 3(a).

As we know, the traditional demodulation method for the frequency-modulated signals has high power consumption and it is difficult to be afforded by the backscatter tag. At the same time, the demodulation method for the amplitude-modulated signals is much more power-efficiency since that the amplitude signals can be captured directly with the passive envelope detector. Therefore, a naive idea is whether we can convert the frequency-modulated signal into an amplitude-modulated signal for demodulation, as shown in Figure 3(b), thus significantly reducing the power consumption.

A. Frequency-Amplitude Transformation

To realize the frequency-amplitude transformation, an intuitive solution is using the frequency selectivity of the filter, such as the RLC filtering circuit [13]. However, the narrow bandwidth of LoRa (*e.g.*, 125/250/500 KHz) renders this idea infeasible. In Saiyan we instead exploit the sharp frequency response of the Surface Acoustic Wave (SAW) filter to transform LoRa chirps into amplitude-modulated signals.

Re-purposing SAW filter as a signal converter. A SAW filter consists of two interdigital transducers (shown in Figure 4). Our design is based on the observation that the frequency response of a SAW filter grows monotonically within a certain frequency band (termed as *critical band*). After passing through the critical band, the chirp signal will be transformed into an AM signal whose amplitude scales with the frequency of this input FM chirp. This allows us to demodulate LoRa chirp by simply tracking the peak amplitude of the AM signal. On the other hand, since SAW filter by its own design is battery-free, such frequency-amplitude transformation doesn't incur extra power consumption to backscatter tags.

Insertion loss of the SAW filter. Insertion loss is a measure of how much the filter attenuates a signal at a given frequency.

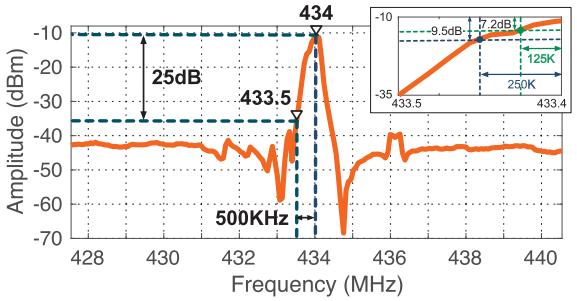

Fig. 5. The amplitude-frequency response of the SAW filter adopted by Saiyan. The central frequency is 434 MHz. The measured insertion loss of this SAW filter is 10 dB. We observe 25 dB, 9.5 dB, and 7.2 dB amplitude variation as the frequency of an incident signal grows from 433.5 MHz, 433.75 MHz, and 433.875 MHz to 434 MHz, respectively.

Numerically, the insertion loss of the SAW filter is the ratio of the signal strength at the input to the filter to the signal strength at the output of the filter. In theory, the insertion loss of the SAW filter is expected to be 6 dB due to the two-stage signal transformation, where the input interdigital transducer transforms electrical signals into acoustic waves; the output interdigital transducer then transforms acoustic waves back into electrical signals. In Saiyan, we take into account the working frequency and bandwidth of LoRa signals and select a general-purpose Qualcomm B3790 [14] SAW filter as the signal converter. Figure 5 shows its frequency response. We observe its insertion loss is measured at 10 dB. This discrepancy arises from the observed signal attenuation of 10 dB at the resonance frequency of 434 MHz.

Amplitude conversion gain after frequency-amplitude transformation. As shown in Figure 5, the signal amplitude grows by 25 dB as the frequency of the incident signal scales from 433.5 MHz to 434 MHz (500 KHz bandwidth of LoRa signals). That means the amplitude conversion gain brought by the frequency-amplitude transformation is 25 dB. To validate this 25 dB amplitude gap is strong enough for differentiating LoRa chirps, we feed four different chirp symbols into this SAW filter and plot the output in Figure 6. Evidently, these symbols peak their amplitude at clearly different time points, confirming the effectiveness of the SAW filter.

B. Demodulation

The transformed symbols are down-converted to the baseband through an envelope detector. Before demodulation, the standard LoRa receiver first digitizes these baseband signals using an ADC, which is power intensive. To save power, an intuitive solution is to replace the ADC with a low-power voltage comparator [15], [16]. The threshold of this comparator is set to a value slightly lower than the peak amplitude of the basband signal. This allows us to locate the peak amplitude by checking the comparator's output. Unfortunately, due to the in-band interference and hardware noise, the transformed AM signal may experience multiple amplitude peaks and valleys that may confuse the comparator.

In Saiyan we instead adopt a **double-threshold based comparator** to stabilize the output binary sequence. After quantization, the MCU coupled with a low-power voltage sampler (counter) decodes each LoRa chirp by localizing the bit

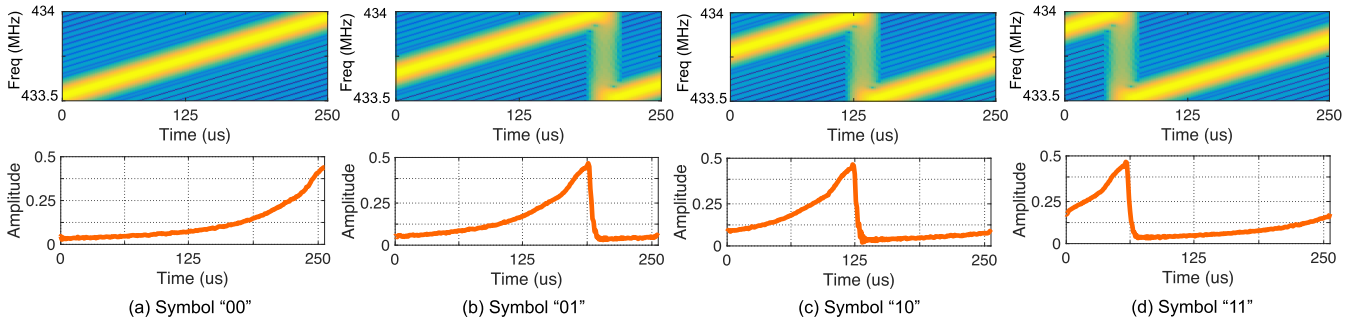

Fig. 6. The input (top) and output (bottom) signals of the SAW filter. The amplitude of the output signal scales with the frequency of the input signal. They reach the maximal value simultaneously.

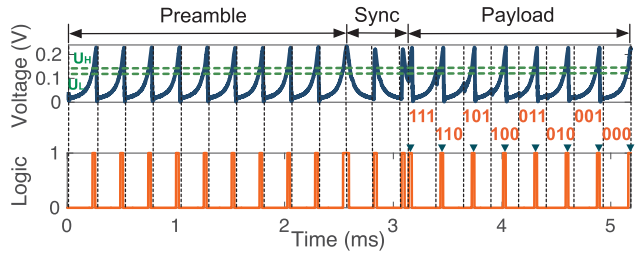

Fig. 7. The decoding process of a LoRa packet.

'1' within each LoRa symbol, as shown in Figure 7. The LoRa preamble contains ten identical up-chirps. Upon detecting the LoRa preamble, Saiyan waits for 2.25 symbol times (sync. symbols) and operates demodulation on the payload hereafter. The details of the double-threshold based comparator and the low-power voltage sampler can be found in NSDI version [17].

Determining the voltage thresholds U_H and U_L. Ideally, U_H should be slightly lower than the peak amplitude of the input signal A_{max}. Let G be the gap between A_{max} and the voltage threshold U_H. We have: $G = 20lg(A_{max}/U_H)$. Thus, U_H can be estimated on the basis of the following equation: $U_H = A_{max}/10^{\frac{G}{20}}$. The threshold voltage U_L is set to $U_H - U_F$, where U_F represents the amplitude of the envelope detector's output. The thresholds U_H and U_L are tuned by two adjustable on-board resistors. In practice, considering that A_{max} and U_F both vary with the link distance, we measure these two values offline under different link distance settings and store a mapping table on each tag to facilitate the configuration of U_H and U_L. To alleviate this manual configuration overhead, one could leverage an Automatic Gain Control (AGC) [18], [19] to adapt the power gain automatically.

III. Super Saiyan

Super Saiyan takes the following actions to consistently improve the demodulation sensitivity: i) improving the SNR of baseband chirp signals with a cyclic-frequency shifting circuit, and ii) improving the sensitivity of demodulator with correlation.

A. Cyclic-Frequency Shifting

Understanding the principle of envelope detector. The envelope detector has been widely adopted by low-power RF devices to down-convert the incident signal. However, due to the inherent non-linearity caused by the squaring operation of CMOS devices [20], both the targeted signal (*i.e.*, feedback signals from the LoRa access point) and the RF noises will be down-converted to the baseband. Consequently, the targeted signal becomes even weaker after down-conversion. We explicate this phenomenon using the following example. Let S_{in} be the incident signal: $S_{in} = S_t + S_n$, where S_t and S_n denote the targeted signal and RF noises, respectively. The output signal S_{out} of this envelope detector can be represented by:

$$\begin{aligned} S_{out} = kS_{in}^2 &= k(S_t + S_n)^2 \\ &= kS_t^2 + 2kS_t \cdot S_n + kS_n^2 \end{aligned} \tag{2}$$

where k represents the attenuation factor. The first term S_t^2 on the right side of this equation manifests that the targeted signal S_t is shifted to the baseband through self-mixing. The second and the third terms both indicate the RF noises are shifted to the baseband after mixed with the targeted signal and the noises themselves, respectively, causing strong interference on the baseband.

Cyclic-frequency shifting. In Saiyan we design a low-power circuit to mitigate the SNR loss brought by the envelope detector. The circuit is realized by two RF mixers and two clock signals. Its operation is detailed as follows.

• **Step 1**. The micro-controller first generates a clock signal $CLK_{in}(\Delta f)$ and mixes it with the incident signal $S(F)$, resulting in two sideband signals $S(F-\Delta f)$ and $S(F+\Delta f)$, as shown in Figure 8(a)-(b). The sideband signals and the incident signal are then down-converted to the intermediate frequency (IF) band (denoted by $S(-\Delta f)$ and $S(\Delta f)$) and the baseband (denoted by $S(0)$) respectively with an envelope detector (Figure 8(c)).

• **Step 2**. Since RF noises are not down-converted to the IF band by the envelope detector, we amplify the unpolluted IF signal $S(\Delta f)$ using a low-power IF amplifier. The frequency selectivity of this IF amplifier filters out signals at other frequencies (*e.g.*, $S(0)$), as shown in Figure 8(d).

• **Step 3**. The power-amplified IF signal $S(\Delta f)$, mixed with another clock signal $CLK_{out}(\Delta f)$, is shifted back to the baseband, as shown in Figure 8(e). At the same time, the noisy baseband signal $S(0)$ will be shifted to the IF band and then filtered by a low-pass filter (Figure 8(f)).

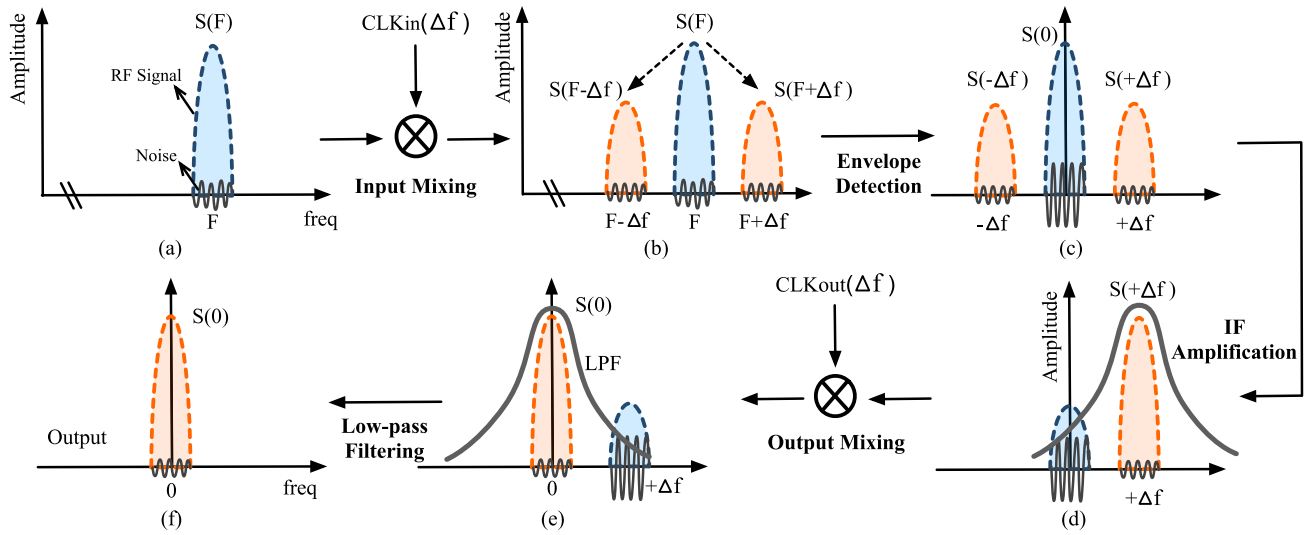

Fig. 8. The illustration of the cyclic-frequency shifting. (a) The input signal $S(F)$. (b) $S(F)$ is first mixed with the clock signal, resulting in two sideband signals $S(F-\Delta f)$ and $S(F+\Delta f)$. (c) The envelope detector extracts the envelope of those three signals and down-converts them to the baseband. (d) The IF amplifier boosts the power of $S(\Delta f)$ and attenuates the power at other frequency bands. (e) The desired signal $S(\Delta f)$ with significantly lower noises is shifted back to the baseband. (f) The output signal $S(0)$.

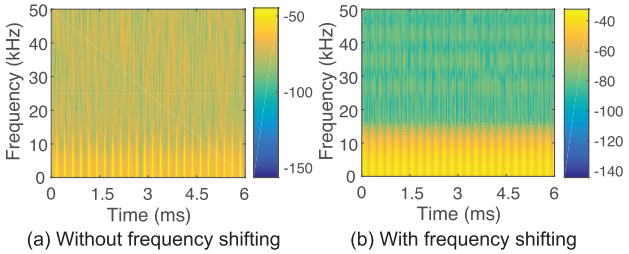

Fig. 9. The spectrum of an incident LoRa signal when being down-converted into the baseband with an envelope detector. (a) Without cyclic-frequency shifting. (b) With cyclic-frequency shifting. The LoRa signal contains 24 LoRa chirps (BW=500KHz, SF=8).

In a nutshell, this circuit first moves the targeted signal to an intermittent frequency band (step 1) to avoid the RF noise contamination introduced by the envelope detector. This also leaves us an opportunity to remedy the SNR loss in down-conversion (step 2). Finally, the targeted signal is moved back to the baseband for demodulation. At the same time the DC offset, flicker and other noises are moved to the IF band and removed by a low-pass filter (step 3).

SNR gain brought by the cyclic-frequency shifting circuit. Our quantitative measurement shows that the cyclic-frequency shifting circuit brings in 11 dB SNR gain. Although the signal centered at $S(F+\Delta f)$ is much lower than the signal centered at $S(F)$ after the up-conversion (step 1), we amplify the signal centered at $S(F+\Delta f)$ using an IF amplifier to compensate for the signal loss caused by the up-conversion (step 2). Figure 9 shows the spectrums before and after feeding the chirp signal into the cyclic frequency shifting circuit. Evidently, both the in-band and out-of-band RF noises have been cleaned by the circuit, ensuring the decodability of chirp signals.

Clock signal generation. The above circuit design relies on two clock signals $CLK_{in}(\Delta f)$ and $CLK_{out}(\Delta f)$. To save power, we program the MCU to generate $CLK_{in}(\Delta f)$ signal and then leverage a delay line to copy $CLK_{in}(\Delta f)$ as $CLK_{out}(\Delta f)$:

$$CLK_{out}(\Delta f) = CLK_{in}(\Delta f + \Delta\phi) \tag{3}$$

where $\Delta\phi$ is the phase shift caused by the delay line. We tune the length of this delay line to ensure $cos(\Delta\phi) \approx 1$ so that $CLK_{out}(\Delta f)$ equals $CLK_{in}(\Delta f)$.

B. Correlation

While the above cyclic-frequency shifting circuit successfully improves the SNR of the incident signal, the demodulation accuracy still suffers degradation when the incident signal is too weak, *e.g.*, close to the noise floor. We thus employ correlation — a mainstream approach that has been largely adopted for packet detection to further improve the demodulation sensitivity. It operates by correlating signals samples with a local chirp template. An energy peak shows up as long as the incident signal matches the template. The receiver then tracks the energy peak and demodulates the incident signal.

C. Overall SNR Gain Analysis

Our demodulation method attains a SNR gain of 30 dB compared to the traditional envelope detector. This substantial improvement primarily results from three key components: the low noise amplifier (LNA) which amplifies the incident signal received by the antenna by 13 dB; the cyclic frequency shift circuit that contributes a gain of 11 dB; and the correlation algorithm further enhances the gain by 6 dB.

IV. Integrating Saiyan Into LoRa Backscatter Tag

As an ultra-low-power demodulator (*downlink*), Saiyan can be integrated with the LoRa backscatter modulator (*uplink*) to enable re-transmission, channel hopping, rate adaption, *etc.*, PHY-layer operations that are important to channel efficiency

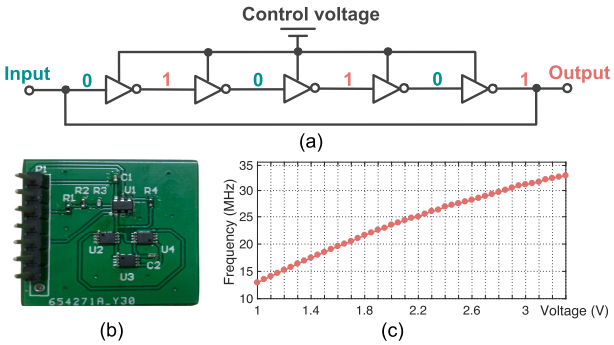

Fig. 10. Illustration of the ring oscillator. (a) Schematic. (b) Hardware prototype. (c) Output frequency vs. control voltage.

yet unavailable on existing LoRa backscatter systems. In this section, we describe how to modulate data on the top of LoRa carriers and how to put the downlink demodulation and uplink modulation together.

A. Uplink Modulation

Taking the LoRa signal as the carrier excitation, our tag conveys data by switching between reflecting and absorbing two states. The backscatter signals will collide with carrier signals when they are transmitting in the same frequency band. To avoid such interference, we plan to shift the backscatter signal to a non-overlapping frequency band. Conventional frequency shifting methods heavily rely on power-consuming hardware components such as high-precision clocks [21] and phase lock loop [22]. On the other hand, due to the dynamic interference in the environment, we expect that the backscatter tag can adaptively switch to different channels to minimize interference. Based on the above dual requirements, we adopt ring oscillator, an ultra-low power oscillator to achieve flexible frequency shifting.

Frequency shifting with a ring oscillator. A ring oscillator consists of an odd number of inverters in a loop with the output of the last stage inverter fed back to the input of the first, as shown in Figure 10(a). Since the output signal of the last stage inverter has a reversed logic as the input of the first stage inverter, the circuit oscillates continuously. The frequency of the ring oscillator is determined by the delay of each inverter which can be further controlled by the input voltage to this ring oscillator. Figure 10(b) shows our ring oscillator prototype consisting of three TI SN74AUP3G04 low-power triple inverter gate [23]. We measure its frequency output at different input voltage settings and show the results in Figure 10(c). As expected, different input voltages correspond to different output frequencies. Hence, one can generate flexible frequency shifting by varying the input voltage As the inverter is extremely low power (*i.e.*, its dynamic current is less than 0.9 μA), the power consumption of this ring oscillator is 10.6 μW, 2,264$\times$ lower than most active radios [24].

Comparison with FS-backscatter [25]. Saiyan and FS-backscatter [25] both leverage the ring oscillator to generate the frequency shifting signals. While FS-backscatter generates a fixed frequency shifting of 20 MHz, Saiyan offers flexibility by allowing the generation of various frequency shifting signals through the adjustment of the bias voltage in the ring oscillator. Compared to the FS-backscatter, Saiyan's uplink supports to adaptively shift the backscatter signal across different frequency bands. This adaptability serves to mitigate the in-band interference effectively.

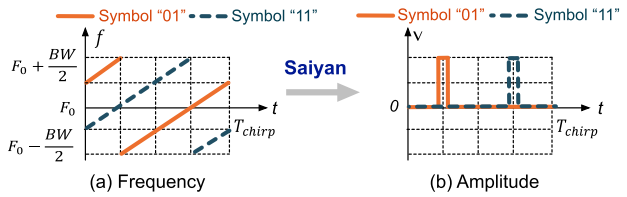

Fig. 11. Parallel demodulation of LoRa signals. The frequency domain features of multiple parallel LoRa signals will be transformed into amplitude features in time domain.

Uplink modulation based on ON-OFF Keying (OOK). Our tag conveys information by shifting the ambient LoRa symbols into another frequency band and adopts the ON-OFF keying (OOK) modulation method to encode data bits. The tag modulates the data bits of "1" and "0" by switching the impedance networking between reflecting and absorbing two states. The receiver monitors two channels simultaneously, one for the carrier channel and the other for the backscatter channel. The backscatter data is demodulated as "1" when the received signals at the backscatter channel can be decoded as a LoRa symbol correctly. Otherwise, the backscatter data is demodulated as "0".

B. Integrating Uplink and Downlink Together

As an ultra-low-power peripheral, Saiyan can be integrated into a powerful LoRa backscatter tag with the uplink modulator through ignorable engineering efforts. This simple integration allows our LoRa backscatter tag to demodulate the feedback signals while retaining the modulation capability at the same time. On the software side, we replicate the sampling rate control logic to facilitate the demodulation.

V. MAC Layer Design

We sketch the MAC-layer in this section. The downlink packets can be divided into the following four cases:

One access point→One tag. The backscatter tag will receive the packets from the access point and respond the commands immediately when decoding the downlink packets successfully.

One access point→Multiple tags. All backscatter tags within the radio range will receive and demodulate the downlink packets from the access point. The access point allocates different time slots to different backscatter tags through query messages. These tags abide by the Time Division Multiple Access (TDMA) protocol to transmit backscatter signals.

Multiple access points→One tag. When there are multiple active LoRa access points, these access points also abide by the time-domain ALOHA protocol. However, it does not guarantee the collision-free transmission. Collision happens when multiple access points select the same slot. In this case, Saiyan supports the demodulation of multiple parallel LoRa signals. The frequency domain features of multiple parallel LoRa signals will be transformed into amplitude features in time domain after the demodulation of Saiyan. As shown in Figure 11, two LoRa chirps will reach the maximal peak

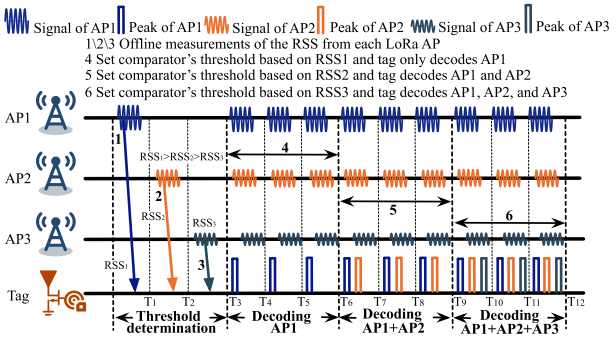

Fig. 12. The illustration of MAC layer operation.

values at different locations when passing through Saiyan. The tag will respond the commands according to priority when decoding the parallel downlink packets successfully.

Multiple access points→Multiple tag. All backscatter tags within the radio range will receive and demodulate the downlink packets from the multiple access points. These access point transmit different commands and query messages to different targeted tags following ALOHA protocol [26], [27], [28]. Similar with the case 2 and 3, different targeted tags will abide by the Time Division Multiple Access (TDMA) protocol to response different query messages from different access points.

Threshold of the comparator in the multiple access points scenario. In scenarios with multiple LoRa APs, we conduct offline measurements of the received signal strength from each LoRa AP individually at the tag. Subsequently, we use the minimum signal strength as the parameter A_{max} in the threshold algorithm mentioned above, allowing us to adjust the thresholds of U_H and U_L dynamically. The tag will observe multiple peaks with different amplitudes and timings. These peaks, influenced by noise signals, pose a challenge for the tag to accurately distinguish between peaks from APs and noise peaks when using the envelope detector and the comparator. We conduct experiments to evaluate the performance of noise on the LoRa parallel decoding (§VII-C). We admit this limitation in our approach. A feasible solution is to utilize a retransmission mechanism. By transmitting the LoRa symbol multiple times, corresponding peaks appear in each decoding window. Since noise exhibits randomness, it fails to produce a consistent peak pattern in each decoding window. As a result, the signal peaks can be identified, enabling the decoding of LoRa symbols even in the presence of a noisy channel.

MAC layer operation. The tag first determines the different thresholds corresponding to decoding different APs, and then leverages the retransmission mechanism to sequentially decode the symbols of different APs. Figure 12 illustrates the MAC layer operation. Taking the decoding of three APs as an example, the tag first measures the received signal strength (RSS) of different APs separately and then obtains the threshold of the comparator corresponding to different APs. Suppose the RSS of three APs is RSS_1, RSS_2, and RSS_3, respectively. These values satisfy that $RSS_1 > RSS_2 > RSS_3$ and the thresholds of the comparator required to decode these three APs also decrease sequentially. After determining

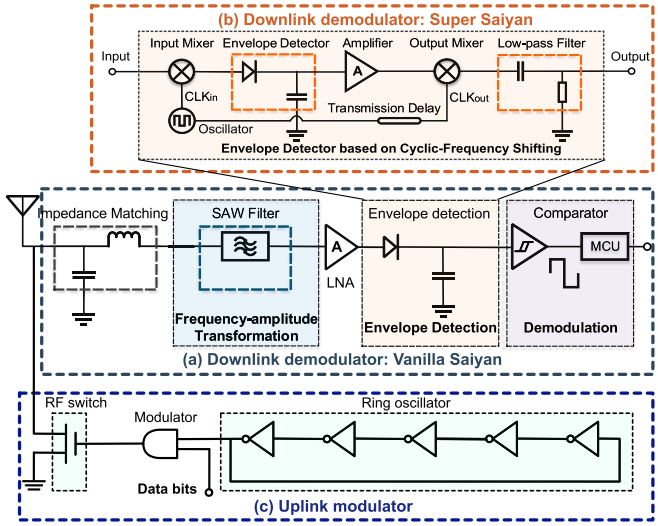

Fig. 13. The schematic of our design. (a) Downlink demodulator of vanilla Saiyan; (b) Downlink demodulator of super Saiyan; (c) Uplink modulator.

the comparator's threshold, the tag begins to decode LoRa symbols. In the first stage, the tag sets the threshold of the comparator corresponding to AP1. We find that only the LoRa symbol of AP1 will have a peak after passing through the comparator, so the LoRa symbol of AP1 can be decoded. We can also leverage the retransmission mechanism to resist noise interference. In the second stage, the tag sets the threshold of the comparator corresponding to AP2, so the LoRa symbols of AP1 and AP2 will have peaks after passing through the comparator. Based on the decoding results of the first stage, the symbol of AP1 can be canceled, and thus the symbol of AP2 can be decoded. Similarly, in the third stage, the tag sets the threshold of the comparator corresponding to AP3, so the LoRa symbols of AP1, AP2, and AP3 will all show peaks after passing through the comparator. Based on the decoding results of the first and second stages, the symbols of AP1 and AP2 can be removed, and thus the symbol of AP3 can be decoded.

VI. Implementation

Figure 13 shows the hardware schematic of our design, including the downlink demodulator of vanilla Saiyan and super Saiyan, and the uplink modulator. We further describe the system implementation in this section.

A. *Downlink Demodulator* Saiyan

Vanilla Saiyan. We implement Saiyan on a 25 $mm\times$ 20 mm two-layer PCB using commercial off-the-shelf analog components and an ultra-low power Apollo2 (10 μA/MHz) [9] MCU. We determine its size through a mixed analytical and experimental approach, striking a balance between the form factor and circuit interference. Saiyan functions with an omni-directional antenna [29] with 3 dBi gain. The incident signal passes through a passive SAW chip B39431B3790Z810 [14] and is transformed into an amplitude-modulated signal. We place a common-gate low-noise amplifier (CGLNA) [30] between the SAW filter and the customized envelope detector to amplify the transformed signal. The amplified signal is then

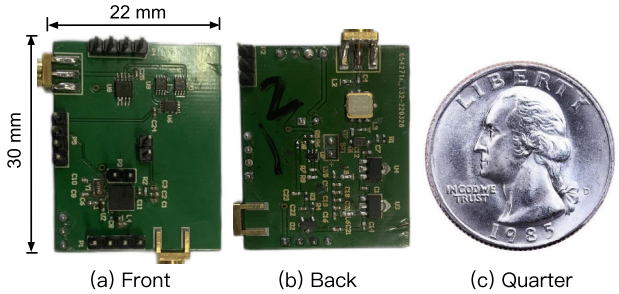

Fig. 14. The hardware prototype of Saiyan. The quarter next to Saiyan demonstrates the form factor.

down-converted to the baseband through the envelope detector. Finally, a low-power voltage comparator NCS2202 [31] is leveraged to quantize the output signal from the envelope detector.

Super Saiyan. We integrate this cyclic-frequency shifting circuit into the envelope detector to construct super Saiyan. It consists of an input mixer, an output mixer, an envelope detector, an IF amplifier, a low-pass filter (LPF), an oscillator, and a transmission line. Specifically, The base clock signal is provided by a micro-power precision oscillator LTC6907 [32]. A low-power transistor 2N222 [33] is adopted as the IF amplifier.

Power management. The energy harvester on Saiyan comprises of a palm-sized photovoltaic panel and a high-efficiency step-up DC/DC converter LTC3105 [34]. It generates 1 mW power every 25.4 seconds in a bright day. The power management module provides a constant 3.3V output voltage to the MCU. The power consumption of this power management module in working mode is approximately 24 μW.

B. Uplink Modulator Based on Ring Oscillator

We use three TI SN74AUP3G04 low-power triple inverter gate [23] to generate the frequency shifting signals from 10 MHz to 25 MHz. A low-power RF switch ADG901 [35] is used as the mixer to backscatter the carrier signals to different frequency band. When Saiyan demodulates the query signal from the LoRa transmitter, the low-power MCU Apollo2 [9] selects the appropriate bias voltage to control the ring oscillator. In this way, the LoRa backscatter tag reflects the carrier signal to the receiver at a clear frequency band.

C. LoRa Transmitter and Receiver

LoRa transmitter.We use two types of LoRa transmitters in the evaluation: i) a LoRa transmitter implemented on a software-defined radio platform USRP N210, and ii) a commercial off-the-shelf LoRa node equipped with a Semtech SX1276RF1JAS [36] chip. Both platforms use a single omni-directional antenna with 3 dBi gain. The transmission power is set to 20 dBm.

LoRa receiver.The LoRa receiver is implemented on a software-defined radio platform USRP N210. We set the sampling rate to 10 MHz, thereby allowing the receiver to monitor six LoRa channels simultaneously. In addition, we admit that our existing backscatter signals based on OOK modulation seems challenging to be directly decoded with commercial devices since that the OOK modulation may alter the structure of LoRa packets and leads to CRC errors. Similar to the some existing backscatter systems [4], [5], we use an USRP device as the receiver to evaluate the performance of the Saiyan's uplink communication. Whereas, our decoding algorithm is independent of hardware platform, which can be implemented on a gateway consisting of a standard Semtech SX1276 LoRa RF-front [24] and a FPGA microprocessor.

D. ASIC Simulation

We simulate the Application Specific Integrated Circuit (ASIC) of Saiyan based on the TSMC 65-nm CMOS process. The active area of on-chip Integrated Circuits (IC) is 0.217 mm^2. The ASIC simulation shows that the power consumption of Saiyan is 93.2 μW. Specifically, the power consumption of LNA, oscillator, and digital circuit is 68.4 μW and 22.8 μW, and 2 μW, respectively. Once Saiyan demodulated the feedback signals, the MCU starts preparing data for packet re-transmissions, which consumes extremely low power (*i.e.*, the power consumption of the ultra-low power Apollo2 [9] in Saiyan is merely 19.6 μW). On the other hand, the ASIC simulation shows that the power consumption of the uplink modulator based on the ring oscillator is only 1.5 μW. Totally, the power consumption of the bi-directional LoRa backscatter tag is around 94.7 μW.

VII. Evaluation

In this section, we present the evaluation results of field studies (§VII-A) and micro-benchmarks (§VII-B). Two case studies follow (§VII-E). Unless otherwise posted, the transmitter and the receiver are collocated throughout the experiment.

Setups. The LoRa transmitter works on the 433.5 MHz frequency band. The spreading factor and the bandwidth are set to 7 and 500 KHz, respectively. The payload of each LoRa packet contains 32 chirp symbols. In each experiment, we let the transmitter transmit 1,000 LoRa packets and then repeat the experiment for 100 times to ensure the statistical validity. We adopt *BER*, *throughput*, and *demodulation range* as the key metrics to assess Saiyan's performance.

- **BER** refers to the ratio of error bits to the total number of bits received by Saiyan.
- **Throughput** measures the amount of received data correctly decoded by Saiyan within one second.
- **Demodulation range** refers to the maximum distance between the tag and the LoRa transmitter when the BER is maintained below 1‰.

A. Field Studies

We conduct field studies both indoors and outdoors to assess the impact of coding rate (CR), spreading factor (SF), and bandwidth (BW) on BER, demodulation range, and throughput, which are three key evaluation metrics.

Impact of coding rate. We place a Saiyan tag 10 m, 20 m, 50 m, 100 m, and 150 m away from a LoRa transmitter. Under each distance setting, we vary the coding rate of LoRa signals and measure BER and throughput. We have three observations based on the results shown in Figure 15(a).

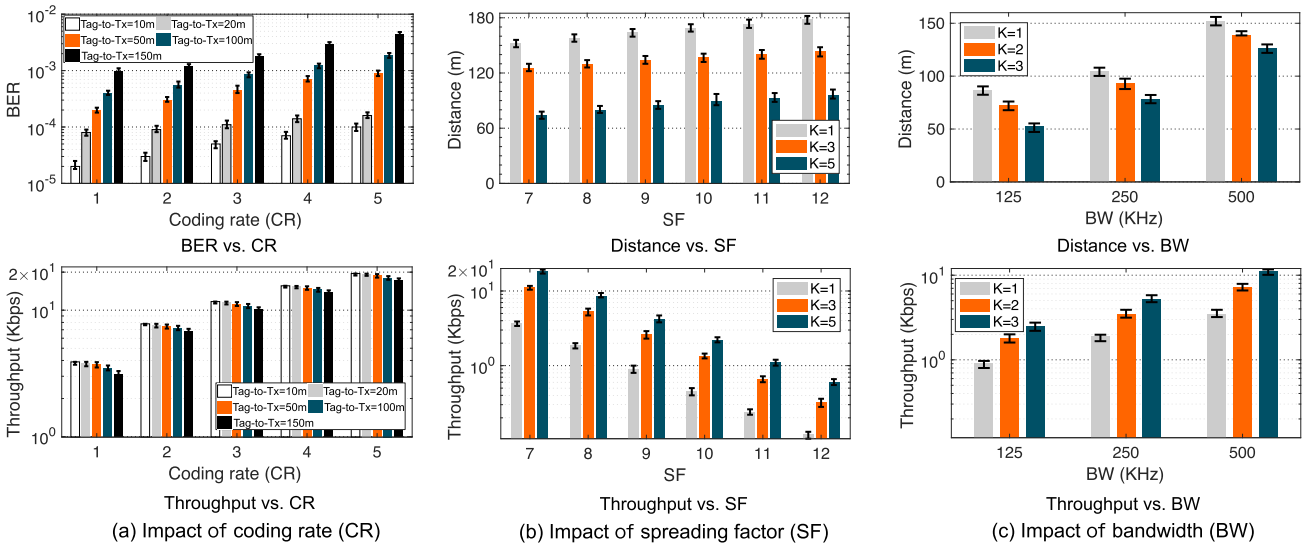

Fig. 15. BER and throughput of Saiyan in different settings. (a) Impact of coding rate (CR). (b) Impact of spreading factor (SF). (c) Impact of bandwidth (BW).

First, the BER grows with the coding rate. As shown in Figure 15(a), the BER under the highest coding rate setting (*i.e.*, 5) is 2.4–5.2× higher than the BER under the lowest coding rate setting (*i.e.*, 1) across all different Tx-to-tag distances. For instance, when the Tx-to-tag distance is 100 m, Saiyan achieves a BER of 1.85‰ under the highest coding rate setting. The BER then drops to 0.4‰ under the same Tx-to-tag distance setting when we change the coding rate to 1. This is expected since the Saiyan tag has to differentiate more types of LoRa chirps under the high coding rate setting.

Second, the throughput grows linearly with the coding rate. For example, when the Tx-to-tag distance is 100 m, the achievable throughput at CR = 5 (18.12 Kbps) is around 5.1× higher than the throughput at a coding rate of 1 (3.57 Kbps).

Third, both the BER and the throughput get exacerbated with the growing Tx-to-tag distance. For instance, when CR = 5, the BER grows dramatically from 0.1‰ to 4.4‰ as the Tx-to-tag distance grows from 10 m to 150 m. The throughput, on the other hand, declines from 19.6 Kbps to 17.2 Kbps. This is expected since Saiyan relies on the signal power to demodulate the incident LoRa signal.

Impact of spreading factor. Next, we vary the spreading factor from 7 to 12 and assess Saiyan's demodulation range and throughput under each setting. The results are shown in Figure 15(b). We observe that the demodulation range grows with the increasing spreading factor. The throughput, on the contrary, declines with the increasing spreading factor. For instance, the demodulation range under the highest spreading factor setting (*i.e.*,SF = 12) is 1.1–1.3× longer than the demodulation range under the lowest spreading factor setting (*i.e.*, SF = 7) across three different coding rate settings. The throughput drops by 30.3–35.1× as we decrease the SF from 12 to 7. This is expected since a higher spreading factor enhances the anti-noise capability of LoRa signals; thus the demodulation range grows. On the other hand, the symbol time grows with the increasing spreading factor, resulting in a lower throughput.

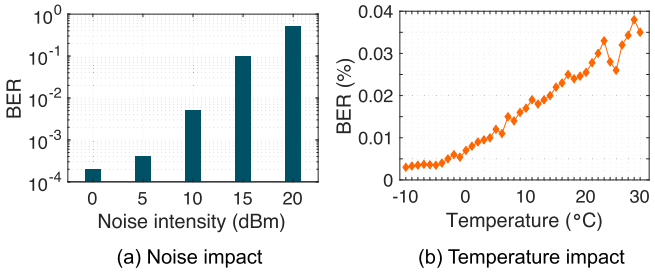

Fig. 16. Saiyan performance under different settings. (a) The impact of noise. (b) The impact of temperature.

Impact of bandwidth. We set the spreading factor to 7 and assess the impact of LoRa bandwidth on the demodulation range and throughput. The results are shown in Figure 15(c). We observe that the demodulation range and the throughput both grow with the LoRa bandwidth. Specifically, given the coding rate of 2, the demodulation range grows from 72.2 m to 138.6 m as we increase the bandwidth from 125 KHz to 500 KHz. On the other hand, since the LoRa symbol time is inversely proportional to the bandwidth, we observe the throughput drops around 4× from 7.2 Kbps to 1.8 Kbps as we decrease the bandwidth from 500 KHz to 125 KHz.

B. Micro-Benchmarks

Impact of noise. We add experiments to thoroughly assess the impact of in-band interference on Saiyan's performance. Two USRP devices were employed, one serving as the LoRa transmitter and the other as the noise generator. The LoRa transmitter sends the LoRa signals with BW of 500 KHz and SF of 7. The transmission power is 20 dBm. The distance from the Saiyan tag to the LoRa transmitter and the distance from the Saiyan tag to the noise generator are both 10 m. We change the power of the noise generator from 0 dBm to 20 dBm and measure the decoding BER at the Saiyan tag. The experiment result is shown in Figure 16(a). The BER grows from 0.02% to 46.5% when the noise intensity increases from

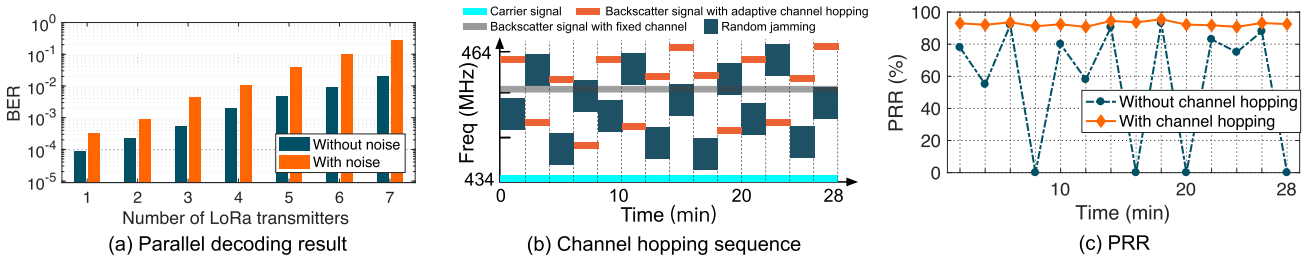

Fig. 17. (a) The parallel decoding result. (b) Adaptive channel hopping sequence. (c) PRR of the LoRa backscatter tag with and without adaptive channel hopping.

TABLE I

ENERGY CONSUMPTION (UNDER 1% DUTY CYCLING) AND COST OF EACH COMPONENT IN Saiyan TAG

Component	SAW Filter	LNA	OSC Clock	Envelope Detector	Comparator	MCU	Total
Energy (μW)	0	248.5	86.8	0	14.45	19.6	369.4
Cost ($)	3.87	4.15	1.25	1.20	1.26	15.43	27.2

TABLE II

ENERGY CONSUMPTION AND COST OF EACH COMPONENT OF THE RING OSCILLATOR-BASED UPLINK MODULATOR

Component	Ring Oscillator	RF Switch	Total
Energy (μW)	11.6	0.5	12.1
Cost ($)	0.42	1.2	1.62

0 dBm to 20 dBm. This experiment shows that the interference signal affects the demodulation performance of Saiyan.

Impact of Temperature. The frequency selectivity of the SAW filter is affected by the ambient temperature. We add experiments to assess the impact of temperature on Saiyan's performance. The result is shown in Figure 16(b). When the temperature varies from -10 °C to 30 °C, the amplitude conversion gain after frequency-amplitude transformation of the SAW filter varies from 0.003% to 0.04%. Although the BER fluctuates with temperature, the BER less than 0.04% indicates that our system can still perfrom well. In addition, the change in amplitude conversion gain is not linear in response to temperature fluctuations. This non-linearity may be attributed to specific characteristics of the SAW filter's structure or material properties.

C. Parallel Demodulation

We deploy multiple LoRa transmitters (1–7) with the power of 20 dBm to examine the parallel demodulation capability of Saiyan. The SF and BW of these LoRa transmitters varies from 7 to 12 and from 125 KHz to 500 KHz, respectively. The distance between each LoRa transmitter and the tag varies from 50 m to 100 m. Then a noise generator sends jamming signals with the power of 10 dBm. The distance between then noise generator and the tag is 50 m. The result is shown in Figure 17(a). We observe the BER is below 0.001 when the number of LoRa transmitters is less than 3. The BER then grows to higher than 0.01 when the number of LoRa transmitters is larger than 5. With the jamming signals, the BER grows by from 0.032% to 27.5% when the number of LoRa transmitters increases from 1 to 7. The high BER is primarily due to the increasing interference in the peak values.

D. Power Consumption & System Cost

Table I summarizes the power consumption (under 1% duty cycling as in LoRa [37]) and cost of each component in Saiyan. Among these hardware components, the most power-hungry parts are LNA and oscillator (OSC) clock, which account for 67.3% and 23.5% of the total power consumption, respectively. As we demonstrate in §VI-D, the power consumption can be effectively reduced by 74.8% when implementing Saiyan on ASIC. Table II summarizes the power consumption and cost of the uplink modulator. The ring oscillator and RF switch only consume 11.6 μW and 0.5μW, respectively. The total consumption of the integrated bi-directional LoRa backscatter tag is 381.5 μW (369.4 μW for Saiyan and 12.1 μW for the uplink modulator). The hardware cost of this LoRa backscatter tag, on the other hand, is around 28.82 USD (27.2 USD for Saiyan and 1.62 USD for uplink modulator), which can be also reduced sharply after Application Specific Integrated Circuit (ASIC) fabrication.

Comparison with the standard LoRa receiver. The demodulation process of a LoRa receiver is as follows. The incoming signal detected by the antenna first goes through an impedance matching circuit. The received signal is amplified by a low noise amplifier (LNA) and then then transformed into an intermediate frequency signal via a mixer. Later, an analog-to-digital converter (ADC) samples these signals at twice the chirp bandwidth, producing discrete I/Q points. Finally, the Fast Fourier Transformation (FFT) operation converts the I/Q samples from the time domain to the frequency domain to decode the LoRa symbols. As illustrated in the datasheet of the LoRa receiver [24], the power consumption of the LoRa receiver is about 19.4–44.4 mW since that the supply voltage is 1.8–3.7 V with the supply current of 10.8–12 mA.

E. Proof-of-Concept Application

Saiyan opens up the first-of-its-kind form of low-power LoRa demodulator for long-range LoRa backscatter communication systems.. In this section, we demonstrate a proof-of-concept application on adaptive channel hopping.

Setups. Our redesigned bi-directional LoRa backscatter tag communicates with the LoRa transmitter/receiver at the 434 MHz frequency band. We put a software-defined radio three meters away from the receiver to randomly jam the channel at different frequency bands. The LoRa receiver monitors the wireless spectrum and notifies the backscatter tag to switch channels in the presence of in-band interference. The backscatter tag generates different frequency shifting via

ring oscillator and backscatters the carrier signal to different channels upon decoding the feedback signals from the receiver. The selected channel sequence of the backscatter tag is shown in Figure 17(b).

Results. Figure 17(c) shows PRR of the LoRa backscatter tag with and without adaptive channel hopping. We can see the PRR is very low when the USRP jams the channel. As the receiver initiates a channel hopping command to the backscatter tag, we witness a significant lift on the PRR. In particular, the median PRR grows to 90.8% to 95.5% once the backscatter tag switches to another channel. This result clearly demonstrates that Saiyan can support better channel utilization through remote control.

VIII. Related Work

We review research topics relevant to Saiyan in this section.

RFID system. A passive RFID tag modulates sinusoidal tone from an RFID reader to transmit data [38]. It can also demodulate amplitude-modulated (AM) signals from a nearby RFID reader [39]. Specifically, the RFID tag down-converts the incident signal to the baseband and accumulates the signal power through an integrator circuit. Subsequently, it compares the accumulated power to a threshold to demodulate incident signals. Saiyan differs from passive RFID tags in two aspects. First, Saiyan demodulates frequency-modulated signal as opposed to amplitude-modulated signal. Second, Saiyan is designed for long-range backscatter systems whereas the passive RFID tag functions within only a few meters.

Ambient backscatter systems. Ambient backscatter systems empower backscatter tags to take the ambient wireless traffic as the carrier signals [16], [40], [41], [42], [43], [44], [45], [46], [47], [48], [49]. For example, WiFi backscatter [40] reuses WiFi signals as the carrier, thereby allowing for the backsactter tag to communicate with a commercial WiFi receiver. Interscatter [50] enables backscatter tags to modulate Bluetooth signals into WiFi signals. LoRa backscatter [6] allows backscatter tags to communicate over long distances by taking advantage of the noise resilience of LoRa symbols. These pioneer works have remarkably improved the throughput and the communication range of backscatter systems. Some recent works support a few types of downlink functionalities such as carrier sensing and packet detection at the packet level. For example, WiFi backscatter [40], Passive-WiFi [51], Interscatter [50], LoRa backscatter [6], and Netscatter [52] use the presence and absence of carrier packets to convey downlink data. However, they cannot demodulate downlink packets at the symbol level, particularly under long-range settings. Saiyan can serve as an important building block to the existing long-range backscatter systems, where the on-demand retransmission is needed due to the drastic packet loss.

Low-power demodulator. With the growth of low-power IoT market, the research community has shifted the focus to the design and implementation of low-power RF receivers, *e.g.*, by replacing the active components with their passive counterparts, or by offloading the power-intensive functions to external devices. Ensworth et al. [53] proposed a 2.4 GHz low-power BLE receiver that offloads the RF local oscillator to an external device. Carlos et al. [54] proposed a low-power 802.15.4 receiver that could demodulate phase-modulated ZigBee signals at orders of magnitude lower power consumption compared with the standard 802.15.4 receiver. However, the working range of this low-power receiver is limited to tens of centimeters, which sets a strong barrier towards the practical deployment. Turbo charging [55] designs a multi-antenna cancellation circuit to facilitate the signal demodulation on backscatter tags. Similarly, full-duplex backscatter [56] enables a backscatter tag to demodulate the instantaneous feedback signal from another backscatter tag. Saiyan differs from these systems in two aspects. First, Saiyan is designed for demodulating frequency-modulated signals as opposed to phase or amplitude modulated signals. Second, Saiyan can support up to 180 m demodulation range, whereas all the aforementioned systems function within only tens of centimeters.

IX. Discussion

Impact of in-band interference on the SAW filter. The in-band interference signal can also be detected by the SAW filter and the envelope detector, potentially leading to a degradation in Signal-to-Noise Ratio (SNR). As demonstrated in Figure 16(a), the in-band interference signal affects the demodulation performance of Saiyan. For higher reliability, the transmitter can repeatedly transmit LoRa symbols multiple times.

Fixed frequency selectivity of the SAW filter. The SAW filter has limited generality from fixed frequency selectivity. To effectively leverage the amplitude-frequency response of the SAW filter for LoRa signal demodulation, it is essential that the frequency of the LoRa signals falls within the operational frequency range of the SAW filter. However, when adopting the channel hopping to solve the interference at the downlink, the LoRa signals may fall outside the 3 dB passband around the resonant frequency of the SAW filter, thus leading to the SNR degradation. In order to address this problem, we can add a frequency shift operation between the impedance matching circuit and the SAW filter. Specifically, the incoming signal detected by the antenna first goes through an impedance matching circuit, then the received signal is mixed with a frequency shifting signal. This ensures that the LoRa signals are shifted to the frequency band which aligns with the response frequency range of the SAW filter. Finally, Saiyan is capable of decoding these frequency-shifted LoRa signals based on the output of the SAW filter. In addition, we can also leverage the ALOHA mechanism among the LoRa APs to alleviate the interference at the tag.

Comparison with other low-power approaches. A simple modulation mechanism such as on-off keying (OOK) [57], [58] or pulse width modulation (PWM) of chirp symbols can also be demodulated with low power consumption. However, compared to the above methods, Saiyan has the following differences. In scenarios where OOK or PWM methods are utilized for transmitting control information from the LoRa AP to the tag, manipulating the signal strength of the LoRa packet becomes necessary. Consequently, a LoRa packet can only transmit one or a few data bits. In contrast, Saiyan can decode each LoRa symbol by transforming its frequency variation to amplitude variation through the SAW filter. Therefore, our

approach enables Saiyan o achieve symbol-level demodulation, providing a higher data rate compared to packet-level OOK or PWM methods.

Limited demodulation range. Saiyan is a low-power LoRa demodulator for the ambient LoRa backscatter system. Saiyan trades-off the LoRa sensitivity and the power consumption and it can supports the Tx-to-Tag distance of 180 m from the LoRa transmitter to the tag. Existing ambient LoRa backscatter, such as PLoRa [4] and Aloba [5], can support a 250 m backscatter range with the Tx-to-Tag distance of only 10 m. The backscatter range significantly drops with the increase of the Tx-to-Tag distance due to the signal attenuation of the carrier signal and the limited reflection efficiency of the tag. The maximum Tx-to-Tag distance of these ambient LoRa backscatters is less than 50 m, which can be covered by Saiyan. Therefore, Saiyan can integrate into these existing ambient LoRa backscatter systems to support the LoRa carrier demodulation.

X. Conclusion

We have presented the design, implementation, and evaluation of Saiyan, the first-of-its-kind low-power demodulator for LoRa backscatter systems. Saiyan leverages the passive SAW filter to achieve the frequency-amplitude transformation directly, reflecting the idea of radio frequency (RF) computing. Saiyan allows that the bi-directional LoRa backscatter tag can realize a plethora of networking functionalities, such as packet re-transmission, channel hopping, and rate adaptation.

References

[1] Y. He, J. Guo, and X. Zheng, "From surveillance to digital twin: Challenges and recent advances of signal processing for industrial Internet of Things," *IEEE Signal Process. Mag.*, vol. 35, no. 5, pp. 120–129, Sep. 2018.

[2] J. Zhang et al., "A survey of mmWave-based human sensing: Technology, platforms and applications," *IEEE Commun. Surveys Tuts.*, vol. 25, no. 4, pp. 2052–2087, 1st Quart., 2023.

[3] *The RF in RFID*. Accessed: 2022. [Online]. Available: https://www.sciencedirect.com/book/9780750682091/the-RF-in-rfid#book-info

[4] Y. Peng et al., "PLoRa: A passive long-range data network from ambient LoRa transmissions," in *Proc. Conf. ACM Special Interest Group Data Commun.*, Aug. 2018, pp. 147–160.

[5] X. Guo et al., "Aloba: Rethinking ON-OFF keying modulation for ambient LoRa backscatter," in *Proc. 18th Conf. Embedded Networked Sensor Syst.*, Nov. 2020, pp. 192–204.

[6] V. Talla, M. Hessar, B. Kellogg, A. Najafi, J. R. Smith, and S. Gollakota, "LoRa backscatter: Enabling the vision of ubiquitous connectivity," in *Proc. ACM UbiComp*, Maui, HI, USA, Sep. 2017, pp. 1–24.

[7] *LoRa Alliance*. Accessed: 2021. [Online]. Available: https://www.lora-alliance.org/

[8] F. Yu, X. Zheng, L. Liu, and H. Ma, "Enabling concurrency for non-orthogonal LoRa channels," in *Proc. ACM MobiCom*, Madrid, Spain, Oct. 2023, pp. 1–15.

[9] *Ultra-Low Power Microcontroller Apollo2 Blue*. Accessed: 2022. [Online]. Available: https://ambiq.com/zh/apollo2-blue/

[10] F. Zhang, F. Yu, X. Zheng, L. Liu, and H. Ma, "DFH: Improving the reliability of LR-FHSS via dynamic frequency hopping," in *Proc. IEEE ICNP*, Reykjavik, Iceland, Oct. 2023, pp. 1–12.

[11] D. Guo, C. Gu, L. Jiang, W. Luo, and R. Tan, "ILLOC: In-Hall localization with standard LoRaWAN uplink frames," in *Proc. ACM UbiComp*, Cambridge, U.K., Sep. 2022, pp. 1–26.

[12] B. Liu, C. Gu, S. He, and J. Chen, "LoPhy: A resilient and fast covert channel over LoRa PHY," in *Proc. 22nd Int. Conf. Inf. Process. Sensor Netw.*, San Antonio, TX, USA, May 2023, pp. 1–13.

[13] *Realization of Differential Circuit*. Accessed: 2022. [Online]. Available: https://en.wikipedia.org/wiki/RLC_circuit

[14] *B39431-B3790-Z810 By Qualcomm-RF360 SAW Filters*. Accessed: 2022. [Online]. Available: https://www.mouser.com/datasheet/2/842/B3790-1092449.pdf

[15] J. R. Smith, A. P. Sample, P. S. Powledge, S. Roy, and A. V. Mamishev, "A wirelessly-powered platform for sensing and computation," in *Proc. ACM UbiComp*, Orange County, CA, USA, Sep. 2006, pp. 39–50.

[16] V. Liu, A. Parks, V. Talla, S. Gollakota, D. Wetherall, and J. R. Smith, "Ambient backscatter: Wireless communication out of thin air," in *Proc. ACM SIGCOMM Conf. SIGCOMM*, Hong Kong, Aug. 2013, pp. 39–50.

[17] X. Guo et al., "Saiyan: Design and implementation of a low-power demodulator for LoRa backscatter systems," in *Proc. USENIX NSDI*, Renton, WA, USA, 2022, pp. 437–451.

[18] B. Reynders et al., "SkySense: Terrestrial and aerial spectrum use analysed using lightweight sensing technology with weather balloons," in *Proc. 18th Int. Conf. Mobile Syst., Appl., Services*, Jun. 2020, pp. 352–363.

[19] X. Cheng, G. Xie, Z. Zhang, and Y. Yang, "Fast-settling feedforward automatic gain control based on a new gain control approach," *IEEE Trans. Circuits Syst. II, Exp. Briefs*, vol. 61, no. 9, pp. 651–655, Sep. 2014.

[20] X. Huang, G. Dolmans, H. de Groot, and J. R. Long, "Noise and sensitivity in RF envelope detection receivers," *IEEE Trans. Circuits Syst. II, Exp. Briefs*, vol. 60, no. 10, pp. 637–641, Oct. 2013.

[21] A. Rokita, "Direct analog synthesis modules for an X-band frequency source," in *Proc. 12th Int. Conf. Microw. Radar.*, Krakow, Poland, 1998, pp. 63–68.

[22] *PLL Synthesizers*. Accessed: 2022. [Online]. Available: https://www.analog.com/en/analog-dialogue/articles/pll-synthesizers.html

[23] *Inverter SN74AUP3G04*. Accessed: 2022. [Online]. Available: https://pdf1.alldatasheetcn.com/datasheet-pdf/view/317334/TI/SN74AUP3G04.html

[24] *Datasheet of the LoRa Receiver SX1276*. Accessed: 2022. [Online]. Available: https://www.mouser.com/datasheet/2/761/sx1276-1278113.pdf

[25] P. Zhang, M. Rostami, P. Hu, and D. Ganesan, "Enabling practical backscatter communication for on-body sensors," in *Proc. ACM SIGCOMM*, Salvador, Brazil, Aug. 2016, pp. 370–383.

[26] X. Zheng, R. Li, Y. Wang, L. Liu, and H. Ma, "Polarscheduler: Dynamic transmission control for floating LoRa networks," *ACM Trans. Sensor Netw.*, vol. 20, no. 67, pp. 1–33, 2024.

[27] Y. Wang, X. Zheng, L. Liu, and H. Ma, "PolarTracker: Attitude-aware channel access for floating low power wide area networks," *IEEE/ACM Trans. Netw.*, vol. 30, no. 4, pp. 1807–1821, Aug. 2022.

[28] F. Yu, X. Zheng, L. Liu, and H. Ma, "LoRadar: An efficient LoRa channel occupancy acquirer based on cross-channel scanning," in *Proc. IEEE INFOCOM*, May 2022, pp. 540–549.

[29] *3dBi Omni-Directional Antenna in 433 MHz*. Accessed: 2021. [Online]. Available: https://www.ebay.com/itm/433Mhz-Magnetic-base-Antenna-3dbi-SMB-Connector-3m-cable-for-Ham-radio-/154317399569

[30] C.-Y. Chiu, Z.-C. Zhang, and T.-H. Lin, "Design of a 0.6-V, 429-MHz FSK transceiver using Q-enhanced and direct power transfer techniques in 90-nm CMOS," *IEEE J. Solid-State Circuits*, vol. 55, no. 11, pp. 3024–3035, Nov. 2020.

[31] *Low-power Comparator NCS2202*. Accessed: 2021. [Online]. Available: https://www.onsemi.com/pub/Collateral/NCS2200-D.PDF

[32] *Silicon Oscillators LTC6907*. Accessed: 2022. [Online]. Available: https://www.analog.com/en/products/ltc6907.html#product-overview

[33] *Low-power Amplifier Transistors 2N222*. Accessed: 2021. [Online]. Available: https://datasheetspdf.com/pdf/490344/Motorola/2N222/1

[34] *Energy Harvesting Chip LTC3105*. Accessed: 2021. [Online]. Available: https://www.analog.com/en/products/ltc3105.html

[35] *RF Switch ADG901*. Accessed: 2021. [Online]. Available: https://www.analog.com/media/en/technical-documentation/data-sheets/ADG901-EP.pdf

[36] *LoRa Transceivers SX1276RF1JAS in 433 MHz*. Accessed: 2021. [Online]. Available: https://www.semtech.com/products/wireless-RF/lora-transceivers/sx1276rf1jas

[37] A. Gamage, J. C. Liando, C. Gu, R. Tan, and M. Li, "LMAC: Efficient carrier-sense multiple access for LoRa," in *Proc. 26th Annu. Int. Conf. Mobile Comput. Netw.*, Sep. 2020, pp. 1–13.

[38] J. Wang, H. Hassanieh, D. Katabi, and P. Indyk, "Efficient and reliable low-power backscatter networks," in *Proc. ACM SIGCOMM Conf. Appl., Technol., Architectures, Protocols Comput. Commun.*, Helsinki, Finland, Aug. 2012, pp. 61–72.

[39] D. Zanetti, B. Danev, and S. Apkun, "Physical-layer identification of UHF RFID tags," in *Proc. ACM MobiCom*, Chicago, IL, USA, Sep. 2010, pp. 353–364.

[40] B. Kellogg, A. Parks, S. Gollakota, J. R. Smith, and D. Wetherall, "Wi-Fi backscatter: Internet connectivity for RF-powered devices," in *Proc. ACM Conf. SIGCOMM*, Chicago, IL, USA, Aug. 2014, pp. 607–618.

[41] D. Bharadia, K. R. Joshi, M. Kotaru, and S. Katti, "BackFi: High throughput WiFi backscatter," in *Proc. ACM Conf. Special Interest Group Data Commun.*, Budapest, Hungary, Aug. 2015, pp. 283–296.
[42] P. Zhang, D. Bharadia, K. Joshi, and S. Katti, "HitchHike: Practical backscatter using commodity WiFi," in *Proc. 14th ACM Conf. Embedded Netw. Sensor Syst.*, Stanford, CA, USA, Nov. 2016, pp. 259–271.
[43] Y. Zou, X. Na, X. Guo, Y. Sun, and Y. He, "TRIDENT: Interference avoidance in multi-reader backscatter network via frequency-space division," in *Proc. IEEE INFOCOM*, Vancouver, BC, Canada, May 2024, pp. 1–10.
[44] X. Guo et al., "Efficient ambient LoRa backscatter with on-off keying modulation," *IEEE/ACM Trans. Netw.*, vol. 30, no. 2, pp. 641–654, Apr. 2022.
[45] X. Guo, Y. He, Z. Yu, J. Zhang, Y. Liu, and L. Shangguan, "RF-transformer: A unified backscatter radio hardware abstraction," in *Proc. 28th Annu. Int. Conf. Mobile Comput. Netw.*, Oct. 2022, pp. 446–458.
[46] H. Jiang, J. Zhang, X. Guo, and Y. He, "Sense me on the ride: Accurate mobile sensing over a LoRa backscatter channel," in *Proc. 19th ACM Conf. Embedded Networked Sensor Syst.*, Coimbra, Portugal, Nov. 2021, pp. 125–137.
[47] C. Li, X. Guo, L. Shangguan, Z. Cao, and K. Jamieson, "CurvingLoRa to boost LoRa network throughput via concurrent transmission," in *Proc. USENIX NSDI*, Renton, WA, USA, Apr. 2022, pp. 879–895.
[48] X. Na, X. Guo, Z. Yu, J. Zhang, Y. He, and Y. Liu, "Leggiero: Analog WiFi backscatter with payload transparency," in *Proc. 21st Annu. Int. Conf. Mobile Syst., Appl. Services*, Helsinki, Finland, Jun. 2023, pp. 436–449.
[49] X. Guo, Y. He, Y. Liu, and L. Shangguan, "A new design paradigm for polymorphic backscatter radios," *GetMobile, Mobile Comput. Commun.*, vol. 27, no. 3, pp. 18–22, Oct. 2023.
[50] V. Iyer, V. Talla, B. Kellogg, S. Gollakota, and J. Smith, "Inter-technology backscatter: Towards internet connectivity for implanted devices," in *Proc. ACM SIGCOMM Conf.*, Salvador, Brazil, Aug. 2016, pp. 356–369.
[51] B. Kellogg, V. Talla, J. R. Smith, and S. Gollakot, "Passive WiFi: Bringing low power to WiFi transmissions," in *Proc. USENIX NSDI*, Santa Clara, CA, USA, Sep. 2018, pp. 151–164.
[52] M. Hessar, A. Najafi, and S. Gollakota, "NetScatter: Enabling large-scale backscatter networks," in *Proc. USENIX NSDI*, Santa Clara, CA, USA, Mar. 2016, pp. 271–284.
[53] J. F. Ensworth, A. T. Hoang, and M. S. Reynolds, "A low power 2.4 GHz superheterodyne receiver architecture with external LO for wirelessly powered backscatter tags and sensors," in *Proc. IEEE RFID*, Phoenix, AZ, USA, May 2017, pp. 149–154.
[54] C. Pérez-Penichet, C. Noda, A. Varshney, and T. Voigt, "Battery-free 802.15.4 receiver," in *Proc. 17th ACM/IEEE Int. Conf. Inf. Process. Sensor Netw. (IPSN)*, Porto, Portugal, Apr. 2018, pp. 164–175.
[55] A. N. Parks, A. Liu, S. Gollakota, and J. R. Smith, "Turbocharging ambient backscatter communication," in *Proc. ACM Conf. SIGCOMM*, Chicago, IL, USA, Aug. 2014, pp. 619–630.
[56] V. Liu, V. Talla, and S. Gollakota, "Enabling instantaneous feedback with full-duplex backscatter," in *Proc. 20th Annu. Int. Conf. Mobile Comput. Netw.*, Hawaii, HI, USA, Sep. 2014, pp. 67–78.
[57] X. Guo, Y. He, and X. Zheng, "WiZig: Cross-technology energy communication over a noisy channel," *IEEE/ACM Trans. Netw.*, vol. 28, no. 6, pp. 2449–2460, Dec. 2020.
[58] X. Guo, Y. He, X. Zheng, L. Yu, and O. Gnawali, "ZigFi: Harnessing channel state information for cross-technology communication," *IEEE/ACM Trans. Netw.*, vol. 28, no. 1, pp. 301–311, Feb. 2020.

Xiuzhen Guo (Member, IEEE) received the B.E. degree from Southwest University and the Ph.D. degree from Tsinghua University. She is currently an Assistant Professor with the College of Control Science and Engineering, Zhejiang University. Her research interests include wireless networks, the Internet of Things, and mobile computing. She is a member of IEEE and ACM.

Yuan He (Senior Member, IEEE) received the B.E. degree from the University of Science and Technology of China, the M.E. degree from the Institute of Software, Chinese Academy of Sciences, and the Ph.D. degree from The Hong Kong University of Science and Technology. He is currently an Associate Professor with the School of Software and BNRist, Tsinghua University. His research interests include wireless networks, the Internet of Things, pervasive, and mobile computing. He is a member of ACM.

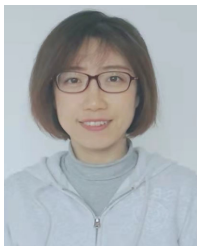

Jing Nan received the B.E. and Ph.D. degrees from Yanshan University, China, in 2001 and 2015, respectively. She is currently an Associate Professor with the School of the Information Science and Engineering, Yanshan University. Her interests include the IoT, full duplex radio, and wireless systems.

Jiacheng Zhang (Student Member, IEEE) received the B.E. degree from Tsinghua University, where he is currently pursuing the master's degree. His research interests include backscatter communication and wireless sensing.

Yunhao Liu (Fellow, IEEE) received the B.S. degree from the Department of Automation, Tsinghua University, and the M.S. and Ph.D. degrees in computer science and engineering from Michigan State University, East Lansing, MI, USA. He is currently a MSU Foundation Professor and the Chairperson of the Department of Computer Science and Engineering, Michigan State University. He also holds the Chang Jiang Chair Professorship at Tsinghua University. His research interests include sensor networks and pervasive computing, peer-to-peer computing, the IoT, and supply chain. He is a Fellow of ACM. He serves as the Editor-in-Chief for *ACM Transactions on Sensor Networks*. He is an ACM Distinguished Speaker.

Longfei Shangguan (Member, IEEE) received the B.E. degree from Xidian University and the Ph.D. degree from The Hong Kong University of Science and Technology. He is currently an Assistant Professor with the Department of Computer Science, University of Pittsburgh. His research interests include networking, the IoT, and wireless systems.